[14] H. Stark and J. W. Woods, *Probability and Random Processes with Applications to Signal Processing*, 3rd ed. Upper Saddle River, NJ: Pearson Edu., 2002.

[15] B. Onaral, K. Pourrezaei, and B. Chance, "Feasibility Study Report for Mobile Warrior System Using Functional Optical Brain Imaging Sensor," Drexel University and University of Pennsylvania, An internal report submitted to Honeywell Inc., Apr. 27, 2004.

A 1.48-mW Low-Phase-Noise Analog Frequency Modulator for Wireless Biotelemetry

Pedram Mohseni* and Khalil Najafi

***Abstract*—This paper presents a low-phase-noise, hybrid LC-tank, analog frequency modulator for wireless biotelemetry employing on-chip NMOS varactors in the inversion region as the frequency tuning element. We demonstrate that a correct estimate for the *destination* signal-to-noise ratio, which quantifies the quality of the wirelessly received signal in a frequency-modulated biotelemetry system, is only achieved after taking into account the *large-signal* oscillation effect on the tank varactor. A prototype chip is fabricated using AMI 1.5-μm double-poly double-metal n-well CMOS process, and exhibits a measured gain factor of 1.21 MHz/V in the mid-range of the tuning voltage and a phase noise of -88.6 dBc/Hz at 10-kHz offset from the 95.1-MHz carrier while dissipating 1.48 mW from a 3 V power supply leading to a figure of merit (FOM) of -166.5 dBc/Hz. The VCO is successfully interfaced with a penetrating silicon microelectrode with 700 μm^2 iridium recording sites for wireless *in vitro* recording of a 50 Hz simulated normal sinus rhythm signal from saline over a distance of ~ 0.25 m. Given a typical gain of ~ 40 dB for fully integrated front-end bioamplifiers, a wireless recording microsystem employing this VCO would be capable of detecting input biopotentials down to the submilivolt range.**

***Index Terms*—Frequency modulation (FM), inversion-mode MOS (I_MOS) varactor, phase noise, wireless biotelemetry.**

I. Introduction

In the past few decades, biomedical microsystems have been extensively utilized for chronic recording of physiological parameters such as heart rate, muscle potential, blood pressure, temperature, and blood flow in both human and animal subjects in health care industry, clinical research, and patient monitoring [1]–[3]. Psychological effects on the subject due to the restriction of motion by cables and leads in tethered measurements in conjunction with the measurement artifacts picked up by the cables can adversely affect these physiological parameters to the extent of rendering the measurement results unreliable. Moreover, the percutaneous leads and cables in implantable biomedical microsystems can cause skin irritation or infection that deteriorates the subject's health condition even further.

Although a wireless link is not a necessary condition for biotelemetric operation, all the aforementioned factors are drawing modern biomedical systems toward wireless technology to remotely measure the physiological parameters as accurately as possible with minimal encumbrance to the subject. Many researchers in the past have utilized fully discrete custom-built frequency modulators operating in the mega-hertz range for remote monitoring of biopotentials in behaving owls [4], freely moving insects [5], [6], and even myelinated axons living in the glass enclosure of a Cone electrode [7]. Nonlinear modulation schemes such as wideband frequency modulation (WBFM) are generally preferred over amplitude modulation (AM) because they can provide significantly improved signal quality in the presence of noise with no increase in the average transmitted power at the expense of increased transmission bandwidth and equipment complexity [8].

Although developing high-performance, high-frequency, and fully integrated voltage-controlled oscillators (VCOs) has always been a focus of active research employing novel RF-CMOS design techniques, most of this effort has traditionally been aimed toward cellular phone network applications in which the performance specifications are significantly more stringent compared to those in biotelemetry. Several researchers have designed CMOS VCOs for frequency synthesis in wireless biotelemetry using ring oscillators [9]–[12]. However, due to the fact that ring oscillators are inherently wide-tunable, they not only have poor phase noise performance but also result in receiver detuning due to excessive carrier frequency deviation when used as analog frequency modulators [12]. In this paper, we present a design alternative employing a low-noise *LC-tank* voltage-controlled oscillator with an on-chip tank varactor as the frequency tuning element. We demonstrate its full functionality in a truly wireless fashion, and highlight the importance of understanding the *large-signal* oscillation effect on the tank varactor. Section II describes the design of the VCO and its integrated varactor while Section III presents the measured results. Finally, Section IV draws some conclusions from this work.

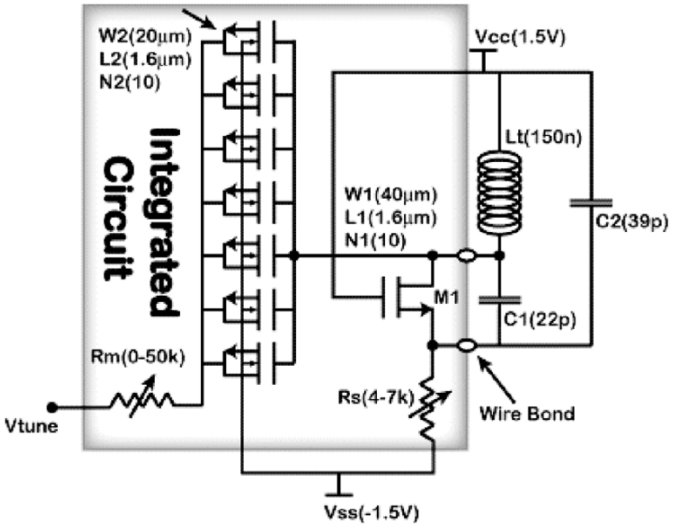

Fig. 1. Schematic of frequency modulator (N is the number of gate fingers).

II. VCO Topology

Fig. 1 shows the circuit schematic of the frequency modulator, which is an LC-tank Colpitts oscillator operating within the frequency band 88–108 MHz, set aside by the United States Federal Communications Commission (FCC) for unlicensed custom-built telemetry intentional radiators for experimentation in educational institutes.[1] Inductor L_t and capacitors C_1, C_2 are external surface mount components (size 0603, Digi-Key, Thief River Falls, MN) that are wire bonded to the integrated

Manuscript received October 29, 2003; revised October 10, 2004. This work was supported in part by the National Institutes of Health (NIH) under Grant R01-DC04198-01. *Asterisk indicates correspponding author.*

*P. Mohseni is with the Center for Wireless Integrated MicroSystems (WIMS), Electrical Engineering and Computer Science Department, University of Michigan, Ann Arbor, MI 48109-2122 USA (e-mail: pmohseni@umich.edu).

K. Najafi is with the Center for Wireless Integrated MicroSystems (WIMS), Electrical Engineering and Computer Science Department, University of Michigan, Ann Arbor, MI 48109-2122 USA (e-mail: najafi@umich.edu)

Digital Object Identifier 10.1109/TBME.2005.845369

[1]http://a257.g.akamaitech.net/7/257/2422/05dec20031700/edocket.access.gpo.gov/cfr_2003/octqtr/pdf/47cfr15.239.pdf.

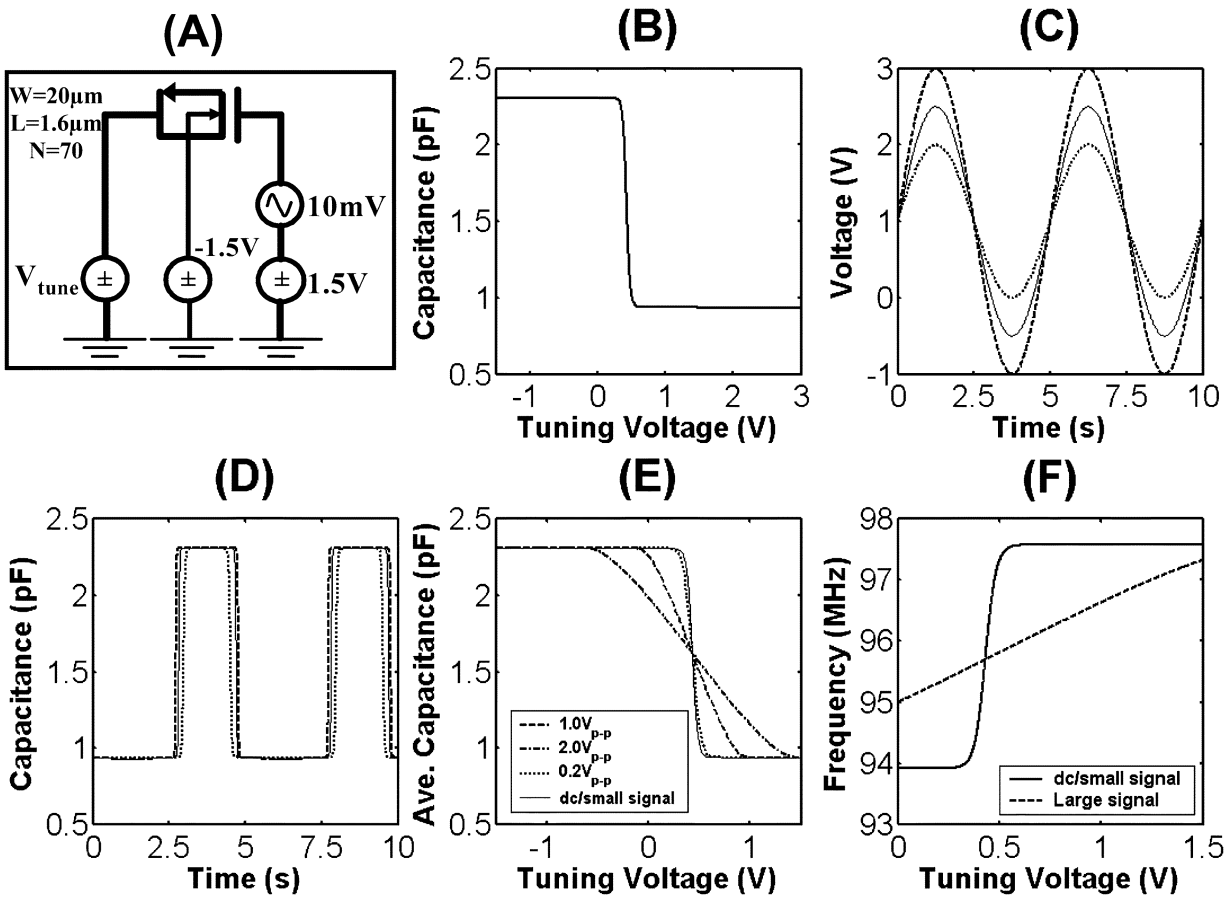

Fig. 2. Large-signal analysis of I_NMOS varactor. (a) Simulated varactor schematic. (b) dc/small signal C–V curve. (c) Large-amplitude oscillation signal across varactor. (d) Time-variant varactor capacitance. (e) Large-signal C–V curves for different oscillation amplitudes superimposed on dc/small signal curve. (f) Simulated frequency tuning curves with small signal (-) and large signal (– - -) varactor operation.

circuit on a custom-designed printed circuit board (PCB). Given the tolerance of the off-chip components ($\pm 5\%$), our simulations reveal that the worst-case carrier frequency change from its nominal value is $\sim 9\%$. Resistor R_s, which is laser programmable in the range of 4-7 $\mathrm{k}\Omega$, sets the bias current, I_{bias}, through transistor M_1. Resistor R_m is also laser programmable in the range of 0-50 $\mathrm{k}\Omega$ in steps of 10 $\mathrm{k}\Omega$. It is set to 10 $\mathrm{k}\Omega$ prior to conducting the measurements in this work.

The implementation of the VCO as an integrated active part interfaced with an external resonator helps to decrease its power consumption, and increase its short term frequency stability by benefiting from the high quality factors (Q) of the off-chip components, which, in turn, makes the design of the on-chip varactor more critical as it affects the overall tank quality factor. Moreover, the telemeter can always be tuned to a higher frequency band such as 174–216 MHz, set aside by FCC for biomedical telemetry devices employed solely on the premises of health care facilities, by selecting lower values for the LC-tank components. However, operation at UHF band such as 900-MHz ISM can potentially be problematic due to spurious series and parallel resonance in addition to the wanted parallel resonance caused by the extra parasitics associated with the IC connection to the external tank and coupling between wire bonds and traces on the external PCB at high frequencies, which can introduce interference into the oscillator or can cause undesired leakage of the large-amplitude oscillation signal to sensitive nodes in other parts of the microsystem [13].

A. MOS Varactors

Many researchers have recently employed MOS varactors in high-frequency integrated VCOs as the frequency tuning element because they are readily available in standard CMOS processes, and are shown to have higher quality factor compared to the commonly utilized diode varactors [14]. MOS varactors are implemented in either the inversion region (I_MOS) or accumulation region (A_MOS). Although no additional fabrication step is required to realize A_MOS varactors, their performance is less characterized or reported by silicon foundries. Therefore, in this work, we have used a programmable-in-size inversion-mode NMOS (I_NMOS) varactor as the frequency tuning element in which the bulk silicon substrate is connected to -1.5 V (see Fig. 1).

Although a MOS capacitor is inherently voltage-dependent, the commonly used C-V curves result from dc/small signal measurements. When the MOS capacitor is incorporated into the VCO, however, the large-amplitude oscillation signal appears across the varactor, and significantly affects the voltage variation of its gate capacitance. This *large-signal* effect has been studied in [15]–[17]. We demonstrate herein that if this large-signal oscillation effect on the LC-tank varactor is overlooked at the design stage, it will lead to gross overestimation of the *destination* signal-to-noise ratio (SNR) (i.e., the average signal-to-noise power ratio at the receiver output) that quantifies the quality of the wirelessly received signal in an FM biotelemetry system.

We first simulated the I_NMOS varactor as shown in Fig. 2(a) using the BSIM3V3.1 transistor model, and derived its dc/small signal C–V curve as depicted in Fig. 2(b). Note that the 1.5-V dc voltage applied to the varactor gate in simulation results from the dc operating point of this node when the varactor is incorporated into the oscillator. In practice, the voltage across the varactor has the following form:

$$V_{\mathrm{var}}(t) = V_{\mathrm{osc}} \sin(\omega_0 t) + V_{\mathrm{tune}} \tag{1}$$

where ω_0 is the oscillation frequency. Fig. 2(c) shows the varactor voltage with V_{tune} set to 1 V and for three different (and equally large)

values of $V_{\rm osc}$ (1, 1.5, and 2 V). As a result, the *instantaneous* value of the varactor capacitance changes significantly during each oscillation period, and is pulse-width-modulated by the large-amplitude oscillation as depicted in Fig. 2(d). An increase in the amplitude of the oscillation signal increases the capacitance pulse widths. Although the time-variant varactor capacitance is a function of the large-amplitude oscillation signal, the *average* capacitance per oscillation cycle still remains a function of the tuning voltage that results in frequency modulation. According to [17], this average capacitance can be written as

$$C_{\rm average}(V_{\rm tune}) \cong \frac{2}{T}\int_0^T C(V_{\rm Var}(t)) \times \cos^2(\omega_0 t)dt \qquad (2)$$

where T is the oscillation period and $C(V_{\rm var}(t))$ is the varactor capacitance as a function of the large-signal varactor voltage. It can be shown that this average capacitance is proportional to the area enclosed by the I–V locus of the varactor subject to the periodic oscillation signal [15]. Equation (2) was numerically calculated for three peak-to-peak oscillation amplitudes of 0.2 V, 1 V, 2 V, and superimposed on the dc/small signal C–V curve in Fig. 2(e). Clearly, as the peak-to-peak oscillation amplitude increases, the *large-signal* C–V curve deviates further from its dc/small signal counterpart with a significant decrease in the rate of varactor capacitance change per tuning voltage. Fig. 2(f) shows the simulated frequency tuning curves assuming both small-signal and large-signal (2.8 V_{p-p} oscillation) operation of the varactor. Clearly, the two curves significantly differ in their shape with the large-amplitude oscillation effectively linearizing the frequency tuning curve. The modulator gain factor, f_Δ, was found to be 34.64 MHz/V and 1.65 MHz/V for the small-signal and large-signal cases, respectively. According to [8], the *destination* SNR of an FM telemetry system is defined as

$$\left(\frac{S}{N}\right)_D = 3\left(\frac{A_m f_\Delta}{W}\right)^2 S_x \gamma \qquad (3)$$

where A_m, W, and S_x are the peak amplitude, maximum frequency component, and normalized energy of the information signal, γ is the output SNR in baseband transmission, and f_Δ is the modulator gain factor. Equation (3) quantifies the superiority of FM transmission compared to the baseband transmission. Therefore, maximizing $(S/N)_D$ is the goal in any FM telemetry system. Clearly, *without* taking into account the large-amplitude oscillation effect on the on-chip varactor, one would overestimate the *destination* SNR by 26.4 dB in this case, which would remarkably compromise the received signal quality after wireless transmission. It should be mentioned that this analysis is independent of the oscillation frequency, ω_0, and solely depends on the large oscillation amplitude. Therefore, the choice of the time scale does not alter the result.

III. Results and Discussion

Individual VCO stages, occupying 0.21 $\rm mm^2$ in die area, were placed near the bond pads in chips fabricated using AMI 1.5 μm double-poly double-metal n-well CMOS process. Fig. 3 shows a microphotograph of the fabricated VCO. Each IC was attached to a custom-designed PCB using conductive epoxy, P-10, (Epoxy Technology, Billerica, MA) after soldering the VCO's three off-chip components in place. The VCO stage was then wire bonded to the PCB with 5 aluminum wire bonds. A short ($\sim$ 2 cm) wire monopole antenna was also soldered in place to radiate the FM signal. The PCB measured 1.7 cm $\times$ 1.2 cm $\times$ 0.16 cm. A fully assembled system weighed 1.1 g including two miniature batteries (*Energizer 337*). A commercially available sensitive FM receiver, WR1550e, (WinRadio Communications, Melbourne, Australia) was used to demodulate the signal after wireless transmission. An 18"-tall stealth mobile antenna with a magnetic base and several feet of RG-174U coax terminated in a standard BNC connector (Grove Enterprises, West Brasstown, NC) was utilized as the receiving antenna. Demodulated signals were displayed using a 500 MHz, 2 GSa/s (Agilent Infiniium, Palo Alto, CA) digital oscilloscope. All the measurements were performed inside a custom-designed Faraday shielding cage (20 in $\times$ 20 in $\times$ 22 in), which was spacious enough to house the receiver antenna while the receiver itself was placed on the bench in the testing laboratory. All the measurements described herein were performed via a wireless link over a distance of $\sim$ 0.25 m.

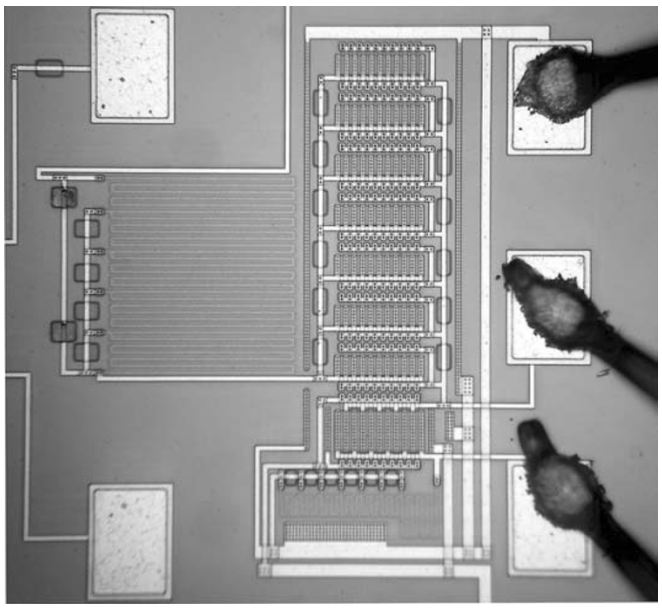

Fig. 3. VCO microphotograph.

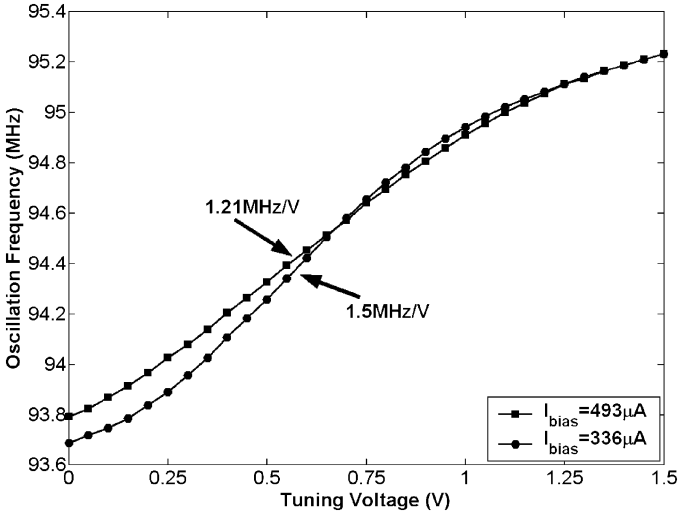

Fig. 4. Measured frequency tuning curves with two different values of $I_{\rm bias}$.

Transistor M_1 had a measured threshold voltage, $V_{\rm th0}$, of $\sim$ 0.55 V and a calculated unity power gain frequency (i.e., maximum oscillation frequency), $f_{\rm max}$, of 7.49 GHz [18]. Fig. 4 shows the measured frequency tuning curves for two different values of $I_{\rm bias}$ obtained by laser trimming resistor R_s. Note the great similarity in shape between these curves and the simulated one with *large-signal* varactor operation [see Fig. 2(f)]. The discrepancy in the operation frequency range was attributed to the fact that the simulation did not fully account for the tank parasitics entailed by the wire bonds, printed circuit board, and tank off-chip components. Nonetheless, this difference was smaller than 2.2% throughout the whole tuning range. Moreover, note that the two measured curves are *different* from each other in shape with larger $I_{\rm bias}$ resulting in lower modulator gain factor in the mid-range of the

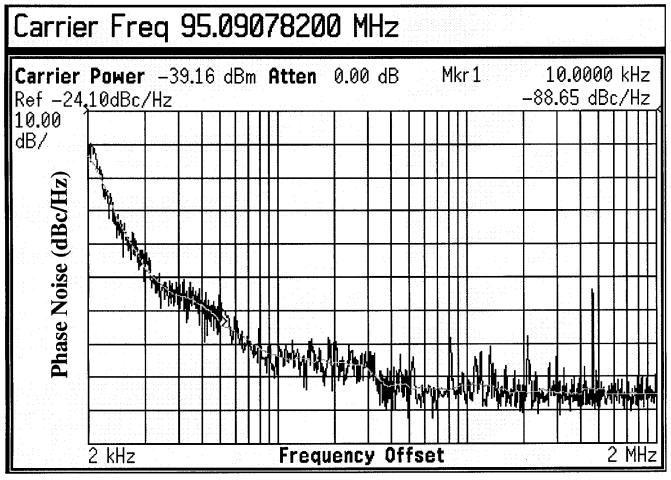

Fig. 5. Measured phase noise of frequency modulator with $V_{\rm tune}$ set to 1.2 V.

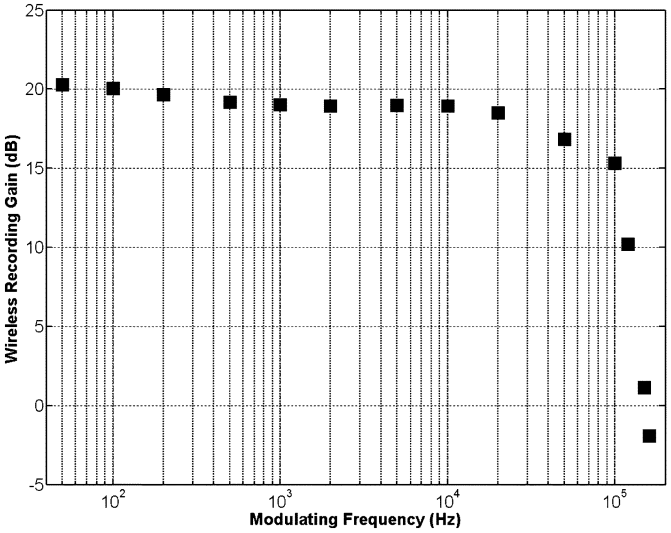

Fig. 6. Measured frequency response of the wireless link. Analog FM is inherently a low-pass process.

tuning voltage. This was attributed to the fact that since the oscillator was operating in the current-limited regime (i.e., the large oscillation amplitude was not limited by the supply voltage) the oscillation amplitude was therefore proportional to $I_{\rm bias}$. Larger oscillation amplitude across the varactor would smooth out its capacitance variation with the tuning voltage [see Fig. 2(e)], which leads to lower modulator gain factor, f_Δ.

Phase noise was measured using an Agilent E4405B spectrum analyzer as shown in Fig. 5. With $V_{\rm tune}$ set to 1.2 V, phase noise was found to be -88.6 dBc/Hz at a frequency offset of 10 kHz from the 95.1-MHz carrier while dissipating 1.48 mW from a 3-V power supply. The widely used figure of merit (FOM) for VCO performance is defined as [13]

$$\mathrm{FOM} = L\{\Delta f\} - 20\log\left(\frac{f_0}{\Delta f}\right) + 10\log\left(\frac{P_{dc}}{1mW}\right) \qquad (4)$$

where $L\{\Delta f\}$ is the measured phase noise at a frequency offset, Δf, from the carrier, f_0, and P_{dc} is the measured dc power dissipation in mW. Based on the measured parameters, the FOM for this VCO was found to be -166.5 dBc/Hz.

To measure the frequency response of the wireless link, we applied a 50 mV_{p-p}, 1-V dc sinusoidal signal to the $V_{\rm tune}$ input using an *Agilent 33250A* function generator, varied its frequency in the range of 0.05–200 kHz, and wirelessly received the sinusoidal signal after demodulation. As shown in Fig. 6, the wireless recording gain was ~ 19 dB at 1 kHz with a 3-dB bandwidth of ~ 70 kHz. According to [8], the transmission bandwidth, B_T, required to transmit a single tone $A_m\cos(\omega_m t)$ is equal to

$$B_T = 2\left(\frac{A_m f_\Delta}{f_m} + 2\right) f_m = 2(\beta + 2) f_m \qquad (5)$$

where f_Δ is the modulator gain factor and β is the single tone modulation index. Analog frequency modulation is inherently a *lowpass* process with higher modulating frequencies (f_m) resulting in lower modulation index (β). This is indeed verified by Fig. 6. Fig. 7(a) shows the wireless reception of a 10 kHz, 50 mV_{p-p} sinusoidal signal. The latency of the wireless link from the input to the output was measured to be $\sim 8\ \mu$s in this case. The required bandwidth to transmit this signal was calculated to be 100.5 kHz according to (5) with f_Δ equal to 1.21 MHz/V. This value increased to 115 kHz at lower power dissipation level of 1 mW.

Finally, we interfaced the VCO stage with a micromachined penetrating silicon microelectrode having 700 $\mu\mathrm{m}^2$ iridium recording sites [19] with an impedance magnitude of 412 k$\Omega\angle$-56° at 1 kHz for wireless *in vitro* recording from saline. The top trace in Fig. 7(b) depicts a 50 Hz, 50 mV_{p-p} simulated normal sinus rhythm input signal to saline

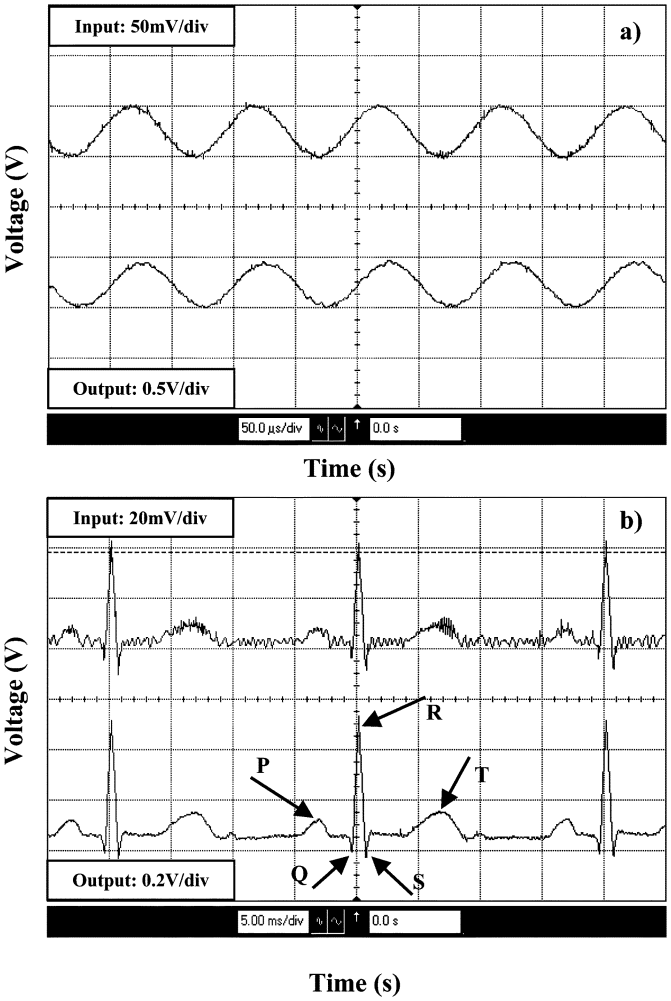

Fig. 7. Wirelessly received waveforms. (a) A 10-kHz single tone modulating signal (top) and wirelessly received signal (bottom). Measured latency is $\sim 8\ \mu$s. (b) A 50-Hz simulated normal sinus rhythm input signal to saline (top) and received signal after wireless *in vitro* recording (bottom).

whereas the bottom trace shows the same signal after wireless transmission. The high-frequency RF noise coupled to the modulating signal from the drain node of transistor M_1 through the gate-source/drain

TABLE I
MEASURED PERFORMANCE OF FREQUENCY MODULATOR FOR WIRELESS BIOTELEMETRY

	This Work	[9]	[10]	[11]
Topology	LC Colpitts	Ring VCO	Ring VCO	Ring VCO
Inductor, Q	Off-chip, >32	-	-	-
Oscillation Freq.	95MHz	200MHz	151MHz	200MHz
Modulation Scheme	Analog FM	QPSK	-	-
Power Dissipation	1.48mW	1.5mW	1.2mW	1.6mW
Phase Noise*	-88.6dBc/Hz @ 10kHz	-82dBc/Hz @ 100kHz	-103.9dBc/Hz @ 500kHz	-80dBc/Hz @ 100kHz
FOM	**-166.5dBc/Hz**	-146.3dBc/Hz	-152.7dBc/Hz	-144dBc/Hz

* @ specified frequency offset from carrier

capacitance of the varactor is attenuated after wireless transmission because analog frequency modulation inherently tends to reject the high-frequency components (see Fig. 6). A 2-point averaging was performed on the received signal upon capturing with the digital oscilloscope to further clean up the output. The wirelessly received output signal fully contained the QRS complex and P, T waves.

Although the input impedance of the VCO stage is high enough to allow its direct interfacing with a nerve recording silicon microelectrode, in practice this VCO should be incorporated into a more complex wireless recording microsystem comprising of fully integrated high-input-impedance front-end bioamplifiers for on-chip ac amplification and dc baseline stabilization [20], [21] followed by a wideband low-output-impedance buffer to drive the VCO. Furthermore, adding clock generation and logic control circuitry for time-division-multiplexing (TDMA) will allow the implementation of a *multichannel* wireless recording microsystem with TDMA/FM communication protocol at the expense of increased power consumption and transmitter/receiver complexity [22]. Given a typical gain of ~ 40 dB for fully integrated bioamplifiers [20], [21] and given the fact that a maximum frequency deviation of 10–50 kHz generally results in good reception in most biotelemetry applications [1], a wireless recording microsystem employing this VCO would be capable of single- or multi-channel detection of input biopotentials down to the submilivolt range [22]. Table I summarizes the measured performance characteristics of the VCO, and compares it with that in the published work. Performance characteristics were not fully reported in [12].

IV. CONCLUSION

We presented a low-phase-noise, hybrid LC-tank, analog frequency modulator for wireless biotelemetry applications employing on-chip inversion-mode NMOS varactors as the frequency tuning element. We demonstrated that if the large-amplitude oscillation effect on the tank varactor is overlooked, it will lead to gross overestimation of the *destination* SNR, which quantifies the quality of the wirelessly received signal in an FM biotelemetry system. A prototype chip was fabricated using AMI 1.5 μm 2P2M n-well CMOS process. It exhibited a measured gain factor of 1.21 MHz/V and a phase noise of -88.6 dBc/Hz at 10 kHz offset from the 95.1-MHz carrier while dissipating 1.48 mW from a 3-V power supply leading to an FOM of -166.5 dBc/Hz. The measured latency of the wireless link from the input to the output in transmission of a 10 kHz single tone was ~ 8 μs. We successfully interfaced the VCO with a penetrating silicon microelectrode for wireless *in vitro* recording of a 50-Hz simulated normal sinus rhythm from saline over a distance of ~ 0.25 m.

ACKNOWLEDGMENT

This work made use of Engineering Research Center Shared Facilities supported by the National Science Foundation under award number EEC-0096866.

REFERENCES

[1] H. Filshie, I. J. H. Duncan, and J. S. B. Clark, "Radiotelemetry of avian electrocardiogram," *Med. Biol. Eng. Comput.*, vol. 18, pp. 633–637, Sep. 1980.
[2] T. B. Fryer, H. Sandler, W. Freund, E. P. McCutcheon, and E. L. Carlson, "A multichannel implantable telemetry system for flow, pressure, and ECG measurements," *J. Appl. Physiol.*, vol. 39, no. 2, pp. 318–326, Aug. 1975.
[3] M. Steyaert, S. Gogaert, T. Van Nuland, and W. Sansen, "A low-power portable telemetry system for eight-channel EMG measurements," in *Proc. Annu. Int. IEEE-EMBS Conf.*, vol. 13, 1991, pp. 1711–1712.
[4] A. Nieder, "Miniature stereo radio transmitter for simultaneous recording of multiple single-neuron signals from behaving owls," *J. Neurosci. Meth.*, vol. 101, pp. 157–164, 2000.
[5] P. Mohseni, K. Nagarajan, B. Ziaie, K. Najafi, and S. B. Crary, "An ultralight biotelemetry backpack for recording EMG signals in moths," *IEEE Trans. Biomed. Eng.*, vol. 48, no. 6, pp. 734–737, Jun. 2001.
[6] S. Takeuchi and I. Shimoyama, "A radio-telemetry system with a shape memory alloy microelectrode for neural recording of freely moving insects," *IEEE Trans. Biomed. Eng.*, vol. 51, no. 1, pp. 133–137, Jan. 2004.
[7] P. R. Kennedy, A. Hopper, C. Linker, and S. M. Sharpe, "A system for real time processing of neural signals for use as prosthetic controllers," in *Proc. Annu. Int. IEEE-EMBS Conf.*, vol. 14, Oct. 29–Nov. 1, 1992, pp. 1343–1344.
[8] K. S. Shanmugam, *Digital and Analog Communication Systems*, 1st ed. New York: Wiley, 1979.
[9] R. J. Betancourt-Zamora, A. Hajimiri, and T. H. Lee, "A 1.5 mW, 200 MHz CMOS VCO for wireless biotelemetry," in *Proc. 1st Int. Workshop Design of Mixed-Mode Integrated Circuits and Applications*, Cancun, Mexico, Jul. 28–30, 1997, pp. 72–74.
[10] R. J. Betancourt-Zamora and T. H. Lee, "CMOS VCO's for frequency synthesis in wireless biotelemetry," in *Proc. IEEE Int. Symp. Low-Power Electronics and Design*, Monterey, CA, Aug. 10–12, 1998, pp. 91–93.
[11] ——, "Low phase noise CMOS ring oscillator VCO's for frequency synthesis," in *Proc. 2nd Int. Workshop Design of Mixed-Mode Integrated Circuits and Applications*, Guanajuato, Mexico, Jul. 27–29, 1998, pp. 37–40.
[12] G. A. DeMichele and P. R. Troyk, "Integrated multichannel wireless biotelemetry system," in *Proc. 25th Int. IEEE-EMBS Conf.*, Cancun, Mexico, Sep. 17–21, 2003, pp. 3372–3375.
[13] P. Kinget, *Integrated GHz Voltage Controlled Oscillators*. Norwell, MA: Kluwer, 1999, pp. 355–381.
[14] P. Andreani and S. Mattisson, "On the use of MOS varactors in RF VCO's," *IEEE J. Solid-State Circuits*, vol. 35, no. 6, pp. 905–910, Jun. 2000.
[15] E. Hegazi and A. A. Abidi, "Varactor characteristics, oscillator tuning curves, and AM-FM conversion," *IEEE J. Solid-State Circuits*, vol. 38, no. 6, pp. 1033–1039, Jun. 2003.
[16] J. Maget, M. Tiebout, and R. Kraus, "MOS varactors with n- and p-type gates and their influence on an LC-VCO in digital CMOS," *IEEE J. Solid-State Circuits*, vol. 38, no. 7, pp. 1139–1147, Jul. 2003.
[17] R. L. Bunch and S. Raman, "Large-signal analysis of MOS varactors in CMOS -G_m LC VCO's," *IEEE J. Solid-State Circuits*, vol. 38, no. 8, pp. 1325–1332, Aug. 2003.
[18] Y. Tsividis, *Operation and Modeling of the MOS Transistor*, 2nd ed. New York: McGraw-Hill, 1999.
[19] *Passive Multichannel Recording and Stimulating Electrode Arrays: A Catalog of Available Designs*, Univ. Michigan, Ctr. Neural Commun. Technol., Ann Arbor, 1999, pp. 1–6.

[20] P. Mohseni and K. Najafi, "A fully integrated neural recording amplifier with DC input stabilization," *IEEE Trans. Biomed. Eng.*, vol. 51, pp. 832–837, May 2004.
[21] R. R. Harrison and C. Charles, "A low-power low-noise CMOS amplifier for neural recording applications," *IEEE J. Solid-State Circuits*, vol. 38, pp. 958–965, Jun. 2003.
[22] P. Mohseni and K. Najafi, "Wireless multichannel biopotential recording using an integrated FM telemetry circuit," in *Proc. 26th Annu. Int. IEEE-EMBS Conf.*, San Francisco, CA, Sep. 1–5, 2004, pp. 4083–4086.

Performance Evaluation of Functional Medical Imaging Compression via Optimal Sampling Schedule Designs and Cluster Analysis

Zhe Chen*, David Dagan Feng, Weidong Cai, and Roger Fulton

***Abstract*—In previous work we have described a technique for the compression of positron emission tomography (PET) image data in the spatial and temporal domains based on optimal sampling schedule designs (OSS) and cluster analysis. It can potentially achieve a high data compression ratio greater than 80:1. However, the number of distinguishable cluster groups in dynamic PET image data is a critical issue for this algorithm that has not been experimentally analyzed on clinical data. In this paper, the problem of experimentally determining the ideal cluster number for the algorithm for PET brain data is addressed.**

***Index Terms*—Cluster analysis, functional imaging, imaging compression, optimal sampling schedule, positron emission tomography (PET).**

I. Introduction

For dynamic functional image data, compression can be performed along two major domains: temporal and spatial. For temporal compression, there are two broad methods have been used: OSS [1], and multivariate analysis techniques, such as principal component analysis (PCA) [2]. OSS is model-based, which can reduce the number of time samples required to be equal to the number of model parameters that are being estimated [3]. PCA is model-independent approach, which has been used in dynamic medical modalities for temporal compression to reduce the large data sets to a smaller number of significant channels [2], [4]. For compression along the spatial domain, vector quantization (VQ) using cluster analysis [5] and transform methods using DCT and wavelets are the basic approaches used [6].

Manuscript received November 4, 2003; revised October 10, 2004. This work was supported in part by ARC and HK-RGC Grants. *Asterisk indicates corresponding author*.

*Z. Chen is with the School of Information Technologies, Madisen Building, University of Sydney, Sydney NSW 2006, Australia (e-mail: zhechen@cs.usyd.edu.au).

D. D. Feng is with the School of Information Technologies, University of Sydney, Sydney NSW 2006, Australia. He is also with the Centre for Multimedia Signal Processing (CMSP), the Department of Electronic and Information Engineering, Hong Kong Polytechnic University.

W. Cai is with the School of Information Technologies, University of Sydney, Sydney NSW 2005, Australia.

R. Fulton is with the PET and Nuclear Medicine Department, Royal Prince Alfred Hospital, Sydney NSW 2050, Australia.

Digital Object Identifier 10.1109/TBME.2005.845367

In previous work we have combined the temporal compression algorithm of [1] based on OSS with a spatial domain compression based on cluster analysis [5]. However, the number of clusters used in dynamic positron emission tomography (PET) image data is a critical issue for this algorithm that has not been experimentally analyzed on clinical brain PET data. A sufficient number of clusters is required to ensure that the functional data contained in the dynamic images is adequately represented, however, too many clusters will increasingly reflect the variation in tissue time activity curves (TTACs) due to noise and will increase the heterogeneity in the index image, resulting in increased noise and less scope for compression of the index image. In this paper, this problem of experimentally determining the optimal cluster numbers for this algorithm for PET brain data will be addressed.

II. Materials and Method

A. Three-Stage Compression Approach

This compression scheme [5] includes three stages: dynamic data compression is performed in the temporal domain with an optimal image sampling schedule [1], then cluster analysis is applied to the TTACs of the dataset to reduce the set of temporal frames into a cluster indexed image and TTAC look-up table. The indexed image is finally compressed by applying a Lempel-Ziv-based lossless coding algorithm.

B. Clinical Case Studies

The datasets used to determine the cluster number were clinical brain ^{18}F-*fluoro-deoxyglucose* (FDG)-PET studies of three patients (one epileptic and two normal). The studies had been carried out at the National PET/Cyclotron Center, Taipei Veterans General Hospital, Taiwan using a PC4096-15 WB with an eight-ring, fifteen-slice PET scanner (GE/Scanditronix). This scanner contains 4096 detectors and achieves axial and transaxial resolutions of 6.5 mm full-width at half-maximum at the center of the field of view. Between 200 and 400 MBq (approximately 0.5 mg) of FDG had been injected intravenously and arterial blood sampling (each sample 2–3 ml) commenced immediately thereafter. The dynamic PET data were corrected for attenuation, decay-corrected to the time of injection and reconstructed using filtered back-projection with a Hanning filter. The reconstructed images were 128×128 with pixel size of $2 \times 2\ \mathrm{mm}^2$. The blood samples (each 2–3 ml) were taken at 8×0.25 min intervals for the first 2 min, then at 2.5, 3, 3.5, 7, 10, 15, 20, 30, 60, 90, and 120 min. These samples were immediately placed on ice and the plasma was subsequently used for the determination of plasma FDG and "cold" glucose concentration.

A typical conventional sampling schedule (CSS) consisting of 22 temporal frames was used to acquire the PET projection data. The sampling times for CSS were 10×0.2 min scans, 2×0.5 min scans, 2×1 min scans, 1×1.5 min scan, 1×3.5 min scan, 2×5 min scans, 1×10 min scan and 3×30 min scans. For the OSS with a five-parameter FDG model, five scanning intervals (frames) were used: 1×0.717, 1×2.483, 1×11.250, 1×60.933, and 1×44.617 min scan [1], [8].

C. Performance Evaluation

The fidelity of images decompressed by the algorithm [5] was assessed by comparing the local cerebral metabolic rate of glucose (LCMRGlc) estimates obtained from the compressed and original data. Parametric images of the LCMRGlc were generated using the Patlak Graphical Approach (PGA) [9]. The normalized mean square